IJIE

Journal homepage: http://penerbit.uthm.edu.my/ojs/index.php/ijie

The International Journal of Integrated Engineering

Performance Properties Optimization of Triaxial Ceramic-Palm Oil Fuel Ash by Employing Taguchi Grey Relational Analysis

A Zainudin*, C K Sia, P Ong, O L C Narong, M A Azlan and W K Lee

Faculty of Mechanical and Manufacturing Engineering, Universiti Tun Hussein Onn Malaysia, 86400 Parit Raja, Batu Pahat, Johor, Malaysia

*Corresponding Author

DOI: https://doi.org/10.30880/ijie. 2019.11.01.026
Received 06 September 2018; Accepted 12 December 2018; Available online 30 April 2019

Abstract: The combustion of massive palm oil wastes has led to the production of Palm Oil Fuel Ash (POFA), especially in Malaysia. In this paper, POFA was applied in a triaxial ceramic application as a secondary filler material. Taguchi Grey Relational Analysis (TGRA) was used to distinguish new parameters efficiently. The parameters investigated were the type of POFA, composition of POFA, molding pressure, sintering temperature, and soaking time. Meanwhile, the responses analyzed included shrinkage, water absorption, apparent porosity, bulk density, and flexural strength. The experimental design was applied based on the Taguchi L_{18} orthogonal array after considering five parameters with 2-3 mixed levels. Statistically, sintering temperature was appointed as the most significant parameter for all responses investigated. The TGRA had suggested that the highest performances were obtained at this condition: 15 wt.% of unground POFA, pressed at 2 t, sintered at 1200 °C, and soaked for 300 min. The achievement of responses with optimal parameters were validated by the crystalline phase and morphology analyses using X-ray diffraction (XRD) and scanning electron microscope (SEM) respectively.

Keywords: Triaxial ceramic; Palm Oil Fuel Ash; Taguchi Grey Relational Analysis; Waste material; L_{18} orthogonal array

1. Introduction

Conventional triaxial ceramic contains three main components: plastic component, flux agent, and filler material, which are typically presented by the materials kaolin, feldspar, and quartz, respectively [1]. Plastic component is used to provide plasticity and green strength to the body and act as a binder to shape the product. Flux agent is typically applied to generate low melting phase and help the vitrification. Meanwhile, filler material is used to improve the stability of body by reducing distortions and shrinkage [2]. The common formulation of composition is 25 wt.% of clay, 25 wt.% of silica, and 50 wt.% of feldspar (generally sodium feldspar) for soft porcelain and 50 wt.% of clay, 25 wt.% of silica, and 25 wt.% of feldspar (generally potassium feldspar) for hard porcelain [3,4]. Recently, several industrial wastes have been applied as a secondary raw material in triaxial ceramic applications [5–7]. These waste materials are mostly presented by large silica which is approximately higher than 50 % [6,8–10]. However, all components have been explored by previous researchers and most of the studies present significant effects to the ceramic products studied.

POFA is a daily wastage material in the boiler of palm oil industry, where empty fruit bunches, palm kernel shell, palm mesocarp fiber, and palm kernel cake have been used as combustible materials. The unmanageable portion of POFA to the specific applications produces a larger landfill region, where it creates many serious problems in terms of storage, transportations, and environmental pollution. Also, this POFA has been explored in concrete application. In the literature, POFA has been applied as a filler and pozzolanic material to increase the strength of polymer concrete [11–

*Corresponding author: gd150136@siswa.uthm.edu.my

14] Recently, POFA has also been reported as an additive material in cement to reduce the shielding of electromagnet interference [15–18]. Previously, POFA was explored briefly in ceramic applications, where the potential of POFA was initially studied in terms of POFA layers [19].

Exploring new raw material in an application requires multiple experiments, which is very expensive and time-consuming processes, as all these works need a proper experimental setup and a large quantity of raw material. Several generalized optimization methods have been applied to minimize the number of experiments and thus reduce the total cost and time consumption. Among them, Taguchi method has been assigned as an effective tool to reduce experimental cost [20–22]. In the recent years, Taguchi method has been applied for various applications including in material engineering fields. Researchers have investigated the sintering conditions of high-temperature Co-fired Ceramics on surface roughness, density, and shrinkage by using Taguchi method [23]. Normally, a full factorial design requires $3^3 = 27$ runs, while Taguchi method simply reduces experiment number to nine experiments. Moreover, an investigation into synthesis and characterization of geopolymers by using treated POFA has also been optimized by using Taguchi method [24]. In this geopolymer study, L_{25} layout is used where six levels of full factorial design requires $5^6 = 15{,}625$ runs. So, it is impossible to do these experiment as well as accompanied by very high cost; while using Taguchi method, it only needs 25 runs. One common aspect in all studies about Taguchi method is minor study has been found in material engineering fields especially ceramic material.

The traditional Taguchi method is based on an orthogonal array of the experiment, which provides much reduced variance between the experiment with an optimum set of process control factors, but it is not suitable for optimization of multiple response optimization problems. Hence, TGRA is being introduced by the researchers to overcome those problems. The GRA, a part of grey system theory, was proposed by Deng (1989) as it is a relatively accurate method for multi-objective optimization with at least two responses. In GRA, all responses variables were converted into a single response function - a representative of all desired response characteristics of the process and then that single response function was maximized. TGRA started the analysis with grey relational generation value where it was a normalized response value ranging from zero to one. Recently, Chamoli et al. have optimized the geometric and flow parameters in a heat exchanger tube perforated disk insect using TGRA [25]. Meanwhile, Sahu and Pal have carried out the TGRA on the friction stir welded AM20 magnesium alloy parameters [26]. Similarly, Shinde and Pawar [27], Baruah et. al [28], and Senthilkumar et al. [29] have also applied TGRA in their respective fields.

Generally, POFA is minorly recorded in a triaxial ceramic study compared to another secondary raw material, where it is mostly reported in concrete application. Taguchi design as a generalized optimization method has also been minorly applied in material study. Therefore, present study applies both traditional Taguchi and Taguchi grey relational analysis techniques to optimize the single and multi-objective of triaxial ceramic components. The experiment was conducted by using Taguchi L_{18} orthogonal array layout. Furthermore, the optimal results were validated regarding morphology analysis and a crystalline phase by using the SEM and XRD analysis respectively.

2. Methodologies

2.1 Design of Experiment and Experimental Works

The study applied Taguchi L_{18} orthogonal array as a layout of experimental design as shown in Table 1. Typically, each parameter was selected based on the higher significant level which was appointed in previous findings. Recently, different type of POFA which are UGPOFA, GPOFA, TPOFA, and UPOFA produce different ranges of response for each respective application [12,30–32].Meanwhile, the selection of POFA composition was based on multiple ranges of response were presented by various material composition parameters [33–35]. The forming process also influences technical properties as reported by previous studies [36–38]. Sintering temperature parameter is highly supported by almost all triaxial ceramic works. Meanwhile, soaking time is highly supported by a study of Bernascony et al. (2011) [39]. Experimental works are totally based on the experimental design provided. Firstly, raw materials were prepared. The study applied kaolin, feldspar, and quartz as plastic component, flux agent, and filler material, respectively. Kaolin (grade KM40) was supplied by Kaolin (M) Sdn. Bhd., Malaysia, and both feldspar and quartz were supplied by Sibelco Sdn. Bhd., Malaysia. POFA as secondary filler material was collected from Genting Ayer Hitam Oil Mill, Johor, Malaysia. Previously, POFA has been studied in terms of POFA layer formations [19]. Combination of Layer 3 and Layer 4 of POFA layers have been assigned as significant particle parts for triaxial ceramic application in a group of collected POFA. These two layers have been presented by higher silica content compared to other two layers (Layer 1 and Layer 2). Moreover, Layer 1 and Layer 2 of collected POFA were presented by a large carbon content. That combination was appointed as POFA for further evaluations like chemical composition. Hence, chemical composition of raw materials used are given in Table 2.

Table-1: Layout of experimental design from Taguchi L_{18} orthogonal array [1]

No.	Design parameters					No.	Design parameters				
	A	B (wt.%)	C (t)	D (°C)	E (min)		A	B (wt.%)	C (t)	D (°C)	E (min)
1	UGPOFA	5	2	800	60	10	GPOFA	5	2	1200	300
2	UGPOFA	5	3	1000	180	11	GPOFA	5	3	800	60
3	UGPOFA	5	4	1200	300	12	GPOFA	5	4	1000	180
4	UGPOFA	15	2	800	180	13	GPOFA	15	2	1000	300
5	UGPOFA	15	3	1000	300	14	GPOFA	15	3	1200	60
6	UGPOFA	15	4	1200	60	15	GPOFA	15	4	800	180
7	UGPOFA	25	2	1000	60	16	GPOFA	25	2	1200	180
8	UGPOFA	25	3	1200	180	17	GPOFA	25	3	800	300
9	UGPOFA	25	4	800	300	18	GPOFA	25	4	1000	60

Note: A: Type of POFA; B: Composition of POFA; C: Molding pressure; D: Sintering temperature; E: Soaking time

Table-2: Chemical composition of raw materials

Oxide composition (wt.%)	Kaolin	Feldspar	Quartz	*POFA
Silica oxide (SiO_2)	53.99	69.51	98.40	64.75
Aluminum oxide (Al_2O_3)	41.48	17.71	1.12	7.71
Iron oxide (Fe_2O_3)	1.49	0.39	0.00	6.88
Calcium oxide (CaO)	-	2.73	-	8.65
Magnesium oxide (MgO)	0.49	-	-	3.11
Sodium oxide (Na_2O)	0.00	5.38	-	-
Potassium oxide (K_2O)	2.55	4.27	0.48	8.90

Note: *Selected POFA layers

The first assigned parameter is the type of POFA, where collected POFAs were sieved by 163 µm sieve to form unground POFA (UGPOFA). Some of UGPOFAs were then ground in Planetary Mono Mill Pulverisette 6 classic line – Fritsch machine and sieved with 63 µm sieve to form GPOFA. Table 3 shows the physical properties of raw materials, where particle size of UGPOFA and GPOFA are often used as a reference.

Table-3: Physical properties of raw materials

Properties	Kaolin	Feldspar	Quartz	UGPOFA	GPOFA
Specific surface area (m^2/m^3)	1816256	1856388	1652048	361186	777787
Arithmetic mean diameter (µm)	6.833	8.972	10.166	49.83	26.465
Geometric mean diameter (µm)	5.007	5.870	6.765	34.485	18.946
D_{10} (µm)	1.55	1.33	1.47	9.33	3.44
D_{20} (µm)	0.94	0.80	0.82	0.95	0.76
D_{30} (µm)	1.43	1.27	1.35	2.47	1.64
D_{40} (µm)	2.11	2.08	2.24	5.23	3.29

Note: D represents the diameter of powder particles, and D_{10} means a cumulative 10% point of diameter

The raw materials were then mixed (dry milling) in a Planetary Mono Mill Pulverisette 6 classic line – Fritsch machine. The compositions of the raw materials are given in Table 4, where it is extracted from the level values of second assigned parameter, composition of POFA in Table 1. Specifically, the mixing process was performed in a 250 mℓ grinding bowl with five units of 15 mm grinding ball. It was operated at 250 rpm for 30 min to create a uniform mixture, with evenly distributed particles of numerous sizes.

Table-4: Composition of raw materials

No	Percentage composition of raw materials (wt. %)				
	Kaolin	Feldspar	Quartz	UGPOFA	GPOFA
1	50	25	20	5	-
2	50	25	10	15	-
3	50	25	-	25	-
4	50	25	20	-	5
5	50	25	10	-	15
6	50	25	-	-	25

The mixed raw materials were then dried in an oven at 100 °C for 24 h in a dry-pressing process, where moistures content is perfectly eliminated. The dried mixed raw materials were weighed as 1 g and 10 g for cylindrical pellet and rectangular bar mold, respectively. Dimensions of 13 mm diameter for a cylindrical pellet and 80 mm x 8 mm for a rectangular bar were used, where it was manually pressed by using Hydraulic Carver Press machine at 2-4 t for 2 min of hold times. Specifically, the binders were not applied during this pressing process. The compacted powders were placed in an oven at 100 °C for 24 hours to eliminate the excess moisture content. It was then sintered in an electric Carbolite HTF 1800 furnace at 800-1200 °C for 60-300 min of soaking times. Specifically, it was applied with 5 °C/min of constant heating and cooling rate.

Investigated performance properties were shrinkage, water absorption, apparent porosity, bulk density, and flexural strength. Shrinkage was performed by using Vernier Calipers to measure dimensions of specimens for both before and after the sintering process, and it is mainly performed regarding the ASTM C326 [40]. Meanwhile, three investigated performance properties namely water absorption, apparent porosity, and bulk density were performed based on the Archimedes principle of ASTM C373 [41]. In this work, an analytical balance from XS-64 Mettler Toledo was used as a weightage device and a digital unstirred water bath as a heater. It was mainly used to weigh the dry mass (D), floating in water mass (S), and saturated mass (M). Thus, water absorption, apparent porosity, and bulk density can be calculated. In each set of parameters, five different sintered specimens were prepared to find the average results. Thus, 90 specimens altogether were prepared for each measurement. The measurements applied the cylindrical pellet specimen. The selected molds dimension was 13 mm diameter. Finally, flexural strength test was performed using the Shimadzu Autograph – SPL 10 kN machine. Specifically, span length of 80 mm was used for flexural strength test, where the test was performed according to the ASTM C1161 [42]. Specifically, this flexural strength applied the rectangular bar specimen where its dimension was 80 mm x 8 mm. It was carried out in three-point configuration. The specimen was placed on the support at the central position and a vertical force was applied until it breaks.

The results were statistically analyzed using MINITAB 17 software to develop optimal design parameters. Sets of optimal design parameters were validated by confirmation experiment, where it was performed with similar process but different parameter values. Besides that, sets of optimal design parameter specimens were also validated by additional confirmation experiment, which was crystalline phase and morphology analyses. Crystalline phase identification was performed by XRD (Bruker D8 Advance Series 2), where it was operated at 40 kV and 40 mA using Cu Kα radiation. Furthermore, XRD results were analyzed by EVA software to compute crystalline phases that existed in the respective optimal specimen. Meanwhile, morphology analysis was performed by SEM (Hitachi SU15100), where metallographic process was initially performed. The surface of the optimal specimens was polished with alumina silicate (0.05 µ) after initial grinding with several silicon carbide paper sizes. The polished surfaces were then etched in 10 wt.% hydrofluoric acid solution for 120 s, dried, and coated with a gold sputter coating. Finally, coated samples were inserted to the chamber of SEM machine and image of microstructure was captured and analyzed.

2.2 Overview of Traditional Taguchi and Taguchi Grey Relational Analysis

Each measured performance property was optimized by using traditional Taguchi analysis to distinguish optimal parameter values for each respective objective. Therefore, five sets of analysis were recorded by single objective optimization. Results of performance properties were reported in terms of average value and it was then recorded as a signal to noise ratio (SNR) value. Theoretically, three models of SNR in the Taguchi design were recorded: (a) nominal the best (NB) – to achieve the target with minimum deviation; (b) larger the better (LB) – to maximize the response; and (c) smaller the better (SB) – to minimize the response. In this study, there was no performance property which was subjected to the nominal the best criteria. Shrinkage, water absorption, and apparent porosity were subjected to the smaller the better criteria. Minimum shrinkage value can improve the management of mold dimension in a specimen preparation [1,43]. Then, minimum water absorption and apparent porosity can improve the qualities of products. Meanwhile, bulk density and flexural strength were subjected to the larger the better criteria. Eq. (1) and (2) express the applied formulae to represent SNR for the criteria of 'smaller the better' and 'larger the better,' respectively. The i, n, and y represent the experiment number, number of trials, and mean value of the observed data, respectively.

$$SNR_{SB} = -10 \log \left[\frac{1}{n} \sum_{i=1}^{n} y_i^2 \right] \quad (1)$$

$$SNR_{LB} = -10 \log \left[\frac{1}{n} \sum_{i=1}^{n} \frac{1}{y_i^2} \right] \quad (2)$$

Precisely, these SNR values can be presented directly from MINITAB 17 software. Independent of the responses, a higher SNR values corresponds to a better performance characteristic. The response tables and main effect plots were then developed to provide information about the optimal parameters for each performance property. Traditional Taguchi analysis can obtain optimal parameter from the main effect plot of SNR results. Particularly, this traditional Taguchi analysis was limited to single objective optimization due to a condition of different units applied by respective response In TGRA, each response unit was standardized and can be adjusted by distinguish effect condition. Hence, TGRA was performed for multiple objectives optimization. In this study, five responses were recorded in this GRA. In GRA, all responses values were converted into a single response function, and it was called grey relational grade (GRG) in this study.

In GRA, the analysis started with grey relational generation value where each response values were normalized from zero to one. Eq. (3) and (4) represent the expressions of grey relational generation corresponding to 'smaller the better' and 'larger the better' criterions, respectively. x_{ij} represents the value of grey relational generation of ith response variable in the jth experiment. Meanwhile, Min y_{ij} and Max y_{ij} represent the smallest and the largest response value respectively, of y_{ij} for the ith response variable among j experiments.

$$x_{ij} = \left[\text{Max } y_{ij} - y_{ij}\right] / \left[\text{Max } y_{ij} - \text{Min } y_{ij}\right] \tag{3}$$

$$x_{ij} = \left[y_{ij} - \text{Min } y_{ij}\right] / \left[\text{Max } y_{ij} - \text{Min } y_{ij}\right] \tag{4}$$

The grey relational coefficient (GRC) was then calculated based on the calculated grey relational generation value. Eq. (5) shows the expression of GRC, where X_j is the ideal normalized value i.e. the maximum of the normalized SNR for the jth response variable and ψ is the distinguishing or identification co-efficient, which is used to adjust the difference of the relational coefficient, where ψ ϵ (0,1). ψ generally weakens the effect of $\max_i |X_j - x_{ij}|$ when it gets too big, enlarging the different significance of the relational coefficient. The distinguishing effects were assigned similarly which is 0.2 because five responses were involved. At the end of GRA, GRG was calculated by averaging the GRC as computed in Eq. (6).

$$\xi_{ij} = \frac{\left[min_i \left|X_j - x_{ij}\right| + \psi max_i \left|X_j - x_{ij}\right|\right]}{\left[\left|X_j - x_{ij}\right| + \psi max_i \left|X_j - x_{ij}\right|\right]} \tag{5}$$

$$\gamma = \left(\frac{1}{n}\right) \sum \xi_{ij} \tag{6}$$

The single response function of GRG was then analyzed traditionally, where it is like the process of single objective optimization. The SNR of the 'larger the better' criteria was used for GRG value. Furthermore, optimal parameters were also developed from response table and main effect plot, which were obtained from MINITAB 17 software [44].

3. Results and Discussions

3.1 Development of Optimal Parameters for Single Objective of Each Performance Property

With the Taguchi L_{18} orthogonal array layout, experiments were performed, and the measured performance properties are given in Table 5. Meanwhile, Table 6 records the calculated SNR values, where larger the better criteria were used for SNR of each performance property. No.3 specimen was recorded as the highest achievement because it was presented by the highest SNR values for the four performance properties which was other than shrinkage. The performance properties other than shrinkage was highly based on higher sintering temperature to obtain higher performance. Since that No.3 specimen was sintered at 1200 °C for 300 min of soaking time, the highest achievement should be gained. The best shrinkage specimen was recorded by No.11 specimen. The conditions prepared by No.11 specimen supplied low energy to the atoms due to the sintering process (800 °C and 60 min). Hence, a minimum densification process occurred during the sintering process. So, the dimension of the sintered specimen was minorly changed. It caused minimum shrinkage. On the contrary, higher temperature presented higher shrinkage value because of higher reactivity level achieved. Measured shrinkage values were recorded by the range of 1.3195 and 24.0777%. Then, water absorption, apparent porosity, bulk density, and flexural strength values were recorded by the range of 0.3219-18.4287%, 0.7783-33.0767%, 1.7992-2.4187 g cm^{-3}, and 0.5187-62.0375 MPa, respectively. Mostly, the lowest

performance specimens are recorded by No.11 specimen, where water absorption, apparent porosity, and bulk density are involved. Furthermore, No.11 specimen was also recorded as a low flexural strength specimen, but No.1 specimen presented the lowest values. Previously, No.11 specimen was also reported as the best shrinkage specimen. Hence, the best shrinkage specimens were opposite with the best specimen of other four performance properties.

Table-5: Measured performance properties

No.	Performance properties					No.	Performance properties				
	SH (%)	WA (%)	AP (%)	BD (g/cm3)	FS (MPa)		SH (%)	WA (%)	AP (%)	BD (g/cm3)	FS (MPa)
1	2.590	15.437	28.037	1.828	0.519	10	22.266	9.019	17.861	2.000	61.478
2	15.823	6.052	13.460	2.227	28.644	11	**1.320**	18.429	33.077	1.800	0.995
3	17.882	**0.322**	**0.778**	**2.419**	**62.038**	12	14.797	6.492	14.231	2.199	35.072
4	6.251	12.179	23.702	1.946	0.674	13	2.307	1.744	4.114	2.345	3.307
5	3.791	13.757	26.050	1.896	4.420	14	17.616	0.981	2.030	2.264	48.420
6	16.513	0.625	1.469	2.352	45.152	15	8.756	14.545	27.053	1.867	1.641
7	2.053	13.747	25.070	1.834	1.952	16	24.078	0.405	0.911	2.247	42.416
8	9.595	0.914	1.943	2.128	30.200	17	2.969	12.713	23.806	1.881	1.206
9	3.323	15.177	27.972	1.851	1.294	18	4.755	11.663	22.746	1.950	4.578

Note: SH: Shrinkage; WA: Water absorption; AP: Apparent porosity; BD: Bulk density; & FS: Flexural strength

Table-6: Signal to noise ratio of performance properties

No.	SNR of performance properties (dB)					No.	SNR of performance properties (dB)				
	SH	WA	AP	BD	FS		SH	WA	AP	BD	FS
1	-8.266	-23.771	-28.955	5.238	-5.702	10	-26.953	-19.103	-25.038	6.020	35.774
2	-23.986	-15.638	-22.581	6.955	29.141	11	**-2.408**	-25.310	-30.390	5.102	-0.040
3	-25.049	**9.845**	**2.177**	**7.672**	**35.853**	12	-23.404	-16.248	-23.065	6.846	30.900
4	-15.918	-21.712	-27.496	5.783	-3.423	13	-7.259	-4.832	-12.285	7.401	10.388
5	-11.575	-22.770	-28.316	5.555	12.908	14	-24.918	0.169	-6.151	7.098	33.700
6	-24.357	4.082	-3.342	7.428	33.094	15	-18.846	-23.254	-28.644	5.423	4.302
7	-6.248	-22.764	-27.983	5.268	5.810	16	-27.632	7.853	0.809	7.034	32.551
8	-19.641	0.780	-5.768	6.558	29.600	17	-9.452	-22.085	-27.534	5.487	1.629
9	-10.429	-23.624	-28.934	5.348	2.235	18	-13.544	-21.336	-27.138	5.802	13.214

Note: SH: Shrinkage; WA: Water absorption; AP: Apparent porosity; BD: Bulk density; & FS: Flexural strength

Previously, No.3 specimen was prepared with following parameter condition: 5 wt.% of UGPOFA, pressed at 4 t, sintered at 1200 °C, and 300 min of soaking times. Meanwhile, No.11 specimen was prepared with following parameter condition: 5 wt.% of GPOFA, pressed at 3 t, sintered at 800 °C, and 60 min of soaking times. The parameter conditions of 5 wt.% of UGPOFA, pressed at 2 t, sintered at 800 °C, and 60 min of soaking times were presented by No.1 specimen. The opposite achievement between No.3 and No.11 specimens was caused by sintering temperature, soaking time, and type of POFA because it was prepared adversely in terms of level values. Composition of POFA and molding pressure parameters had minorly changed the achievement properties values.

However, the optimal parameters were not directly obtained from the best specimen of Taguchi L_{18} orthogonal array layout. Response tables and main effect plots were reported to fulfill it, and these reports were automatically given in Taguchi analysis in MINITAB 17 software. Table 7 records the response tables of performance properties. Each property presents different order of significant level of parameters. The highest delta (based on means) values indicated the most significant parameter. Sintering temperature was reported as the most significant parameter for all investigated performance properties. Theoretically, sintering temperature is parallel with mullite phase formation. All investigated performance properties are also highly depending on mullite phase formation, where its difference can influence the responses. Meanwhile, the type of POFA presented as the least significant parameter. The orders of significant level for the second, third, and fourth were differently reported, where only shrinkage, water absorption, and apparent porosity presented similar orders. The second, third, and fourth significant level of shrinkage, water absorption, and apparent porosity were soaking time, composition of POFA, and molding pressure, respectively. For bulk density, the order of second, third, and fourth significant level were composition of POFA, soaking time, and molding pressure, respectively. Meanwhile, for flexural strength, the order of second, third, and fourth significant level were reported as composition of POFA, molding pressure, and soaking time, respectively.

Table-7: Response tables of performance properties

Level	SNR					Mean				
	A	**B**	**C**	**D**	**E**	**A**	**B**	**C**	**D**	**E**
Shrinkage										
1	-16.16	-18.34	-15.38	-10.89	-13.29	8.647	12.446	9.924	4.201	7.474
2	-17.16	-17.15	-15.33	-14.34	-21.57	10.985	9.205	8.519	7.254	13.216
3		-14.49	-19.27	-24.76	-15.12		7.795	11.004	17.991	8.756
Delta	0.99	3.85	3.94	13.87	8.28	2.338	4.651	2.486	**13.790**	5.742
Rank	5	4	3	1	2	5	3	4	**1**	2
Water absorption										
1	-12.841	-15.038	-14.055	-23.293	-14.822	8.690	9.292	8.755	14.747	10.147
2	-13.794	-11.386	-14.142	-17.265	-11.370	8.443	7.305	8.808	8.909	6.765
3		-13.529	-11.756	0.604	-13.762		9.103	8.137	2.044	8.789
Delta	0.953	3.651	2.387	23.897	3.452	0.247	1.987	0.670	**12.702**	3.382
Rank	5	2	4	1	3	5	3	4	**1**	2
Apparent porosity										
1	-19.022	-21.308	-20.158	-28.659	-20.660	16.498	17.907	16.616	27.274	18.738
2	-19.937	-17.706	-20.123	-23.561	-17.791	16.203	14.070	16.728	17.612	13.550
3		-19.425	-18.158	-6.219	-19.988		17.075	15.708	4.165	16.763
Delta	0.915	3.603	2.000	22.440	2.869	0.295	3.838	1.020	**23.109**	5.188
Rank	5	2	4	1	3	5	3	4	**1**	2
Bulk density										
1	6.201	6.305	6.124	5.397	5.989	2.053	2.079	2.033	1.862	2.004
2	6.246	6.448	6.126	6.305	6.433	2.061	2.112	2.032	2.075	2.102
3		5.916	6.420	6.968	6.247		1.982	2.106	2.235	2.065
Delta	0.045	0.532	0.296	1.571	0.444	0.008	0.130	0.074	**0.373**	0.098
Rank	5	2	4	1	3	5	2	4	**1**	3
Flexural strength										
1	15.5017	20.9875	12.5662	-0.1665	13.3460	19.432	31.457	18.391	1.055	16.936
2	18.0464	15.1615	17.8231	17.0600	20.5115	22.124	17.269	18.981	12.995	23.108
3		14.1732	19.9328	33.4286	16.4647		13.608	24.962	48.284	22.290
Delta	2.5447	6.8143	7.3666	33.5951	7.1655	2.691	17.850	6.571	**47.229**	6.172
Rank	5	4	2	1	3	5	2	3	**1**	4

Note: A: Type of POFA; B: Composition of POFA; C: Molding pressure; D: Sintering temperature; E: Soaking time

Response table (based on SNR) values were used to develop main effect plots of all investigated performance properties. Fig. 1 records the main effect plots of performance properties. It presents optimal parameter values for each performance property. Firstly, Fig. 1(a) shows that optimal parameters of the best shrinkage value are recorded as 25 wt.% of UGPOFA, pressed at 4 t, sintered at 800 °C, and 60 min of soaking times. Theoretically, lower shrinkage is achieved when lower sintering temperature is applied. Moreover, it is also achieved when lower soaking time is applied. These two parameters influence the shrinkage values in terms of energy amount [43,45]. Lower sintering temperature and soaking time would supply minimum amount of energy to the specimen's particles. Furthermore, the best shrinkage specimen is also reported by the 25 wt.% of POFA compositions, where it is related to a different of melting point value between POFA and quartz. Previously, POFA was recorded as the lower melting point material compared to quartz. Theoretically, a material with a lower melting point generate lower energy amount and it is distinguished by higher shrinkage value.

Fig. 1(b) shows optimal parameters of the best water absorption, where its optimal parameter values were recorded by a condition of 15 wt.% of UGPOFA, pressed at 4 t, sintered at 1200 °C, and 180 min of soaking times. It was similarly recorded by the best apparent porosity as shown in Fig. 1(c). These two optimal specimens were sintered at the highest sintering temperature, where it generated higher amount of energy to the specimens. The sintering temperature is proportional with driving and external forces values. If higher sintering temperature is involved, higher driving and external forces is confirmed. Fundamentally, sintering is the process of compacting and forming a solid mass of material by heat or pressure without melting it to the point of liquefaction. Higher driving and external forces will be supplying higher compacting and forming process of a solid mass of material. These actions reduce the voids between particles of specimens, where the lower apparent porosity is reached [43,45]. Similar approach is reported by water absorption theory, where the reduction of voids between particles lowers the water absorption values [43,45].

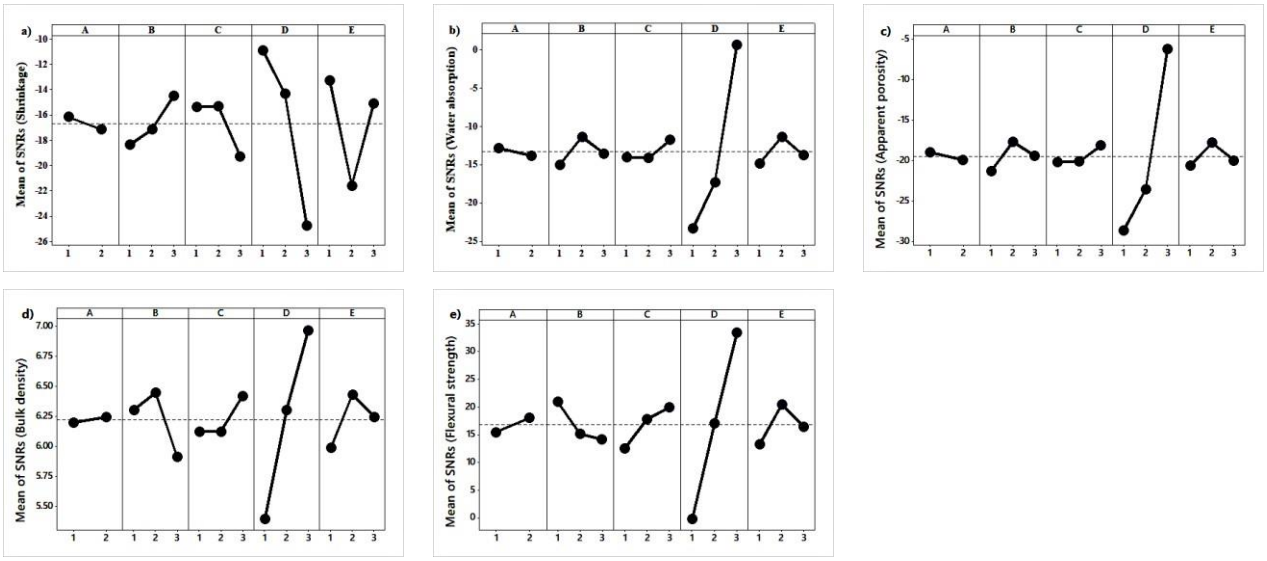

Fig.-1: Main effect plot for signal to noise ratio of following performance properties: a) Shrinkage; b) Water absorption; c) Apparent porosity; d) Bulk density; and e) Flexural strength.

Optimal water absorption and apparent porosity specimens were also recorded by 180 min of soaking times. Particularly, the highest soaking time (300 min) values were expected to achieve the highest performances for these two optimal specimens. It is because higher soaking time value is expected to give longer time for compacting and forming process of a solid mass of material. However, middle values of determined soaking time values were reported by MINITAB 17 software. The 15 wt.% of POFA composition was expected to neutralize the amount of energy during sintering process where lower soaking time was covered by lower composition of POFA. Lower composition of POFA reduced energy of sintering process by higher melting point material and was presented by a few amounts of quartz material.

Optimal parameters of the best bulk density are given in Fig. 1(d), where it was recorded as 15 wt.% of GPOFA, pressed at 4 t, sintered at 1200 °C, and 180 min of soaking times. Excluding the type of POFA, similar optimal parameters were reported for the best bulk density specimen. Furthermore, the type of POFA has been assigned as the least influential parameter for all optimal performance properties. GPOFA was presented by the best bulk density specimen to improve compaction and forming process in sintering process because GPOFA was made by lower particle size than UGPOFA. Theoretically, a smaller particle size powder would be more reactive [46–48].

Fig. 1(e) shows optimal parameters of the best flexural strength, where it was recorded by a condition of 5 wt.% of GPOFA composition, pressed at 4 t, sintered at 1200 °C, and 180 min of soaking times. It was absolutely like optimal bulk density specimen, but composition of POFA 5 wt.% was reported by optimal flexural strength specimen.

3.2 Development of Optimal Parameter for Multiple Objective Specimen

Particularly, each performance property namely shrinkage, water absorption, apparent porosity, bulk density, and flexural strength were recorded by different optimal parameters values. In real life, triaxial ceramic process must be performed at the equivalent level of design and process parameters to get optimization on all responses. The Taguchi GRA is used to perform multiple objectives optimizations. Initially, grey relational generation values are calculated by Eq. (3) and (4), and it was recorded in Table 8. It must be equivalent to SNR values of Table 6.

The GRCs were calculated from Eq. (5), where distinguish effect were assigned as 0.2 for each performance property. Meanwhile, GRG was then calculated from Eq. (6), where Table 9 presents calculated GRC and GRG values. It was included by SNR of GRG values and grey order. From the measured performance properties values until GRC values, the order of the best specimen for each performance property was similar. Particularly, these measured and calculated values were synchronized with each other, where something wrong was expected when some part of these values were not fully synchronized. Furthermore, it must be influencing the GRG values if those values were not synchronized. The best specimen by considering these five performance properties were reported by No.3 specimen, where it was also recorded by single objective optimization which was performance properties other than shrinkage. No.11 specimen was previously recorded as the best shrinkage specimen, but it was ranked as 8th grey order for multiple objectives optimization.

Table-8: Grey relational generation values

No.	Performance properties					No.	Performance properties				
	SH	WA	AP	BD	FS		SH	WA	AP	BD	FS
1	0.94	0.17	0.16	0.05	0.00	10	0.08	0.52	0.47	0.32	0.99
2	0.36	0.68	0.61	0.69	0.46	11	**1.00**	0.00	0.00	0.00	0.01
3	0.27	**1.00**	**1.00**	**1.00**	**1.00**	12	0.41	0.66	0.58	0.65	0.56
4	0.78	0.35	0.29	0.24	0.00	13	0.96	0.92	0.90	0.88	0.05
5	0.89	0.26	0.22	0.16	0.06	14	0.28	0.96	0.96	0.75	0.78
6	0.33	0.98	0.98	0.89	0.73	15	0.67	0.21	0.19	0.11	0.02
7	0.97	0.26	0.25	0.06	0.02	16	0.00	1.00	1.00	0.72	0.68
8	0.64	0.97	0.96	0.53	0.48	17	0.93	0.32	0.29	0.13	0.01
9	0.91	0.18	0.16	0.08	0.01	18	0.85	0.37	0.32	0.24	0.07

Note: SH: Shrinkage; WA: Water absorption; AP: Apparent porosity; BD: Bulk density; & FS: Flexural strength

Table-9: Grey relational coefficient and grey relational grade

Exp.	GRC					GRG	SNR of GRG	Grey Order
	$SH^{0.2}$	$WA^{0.2}$	$AP^{0.2}$	$BD^{0.2}$	$FS^{0.2}$			
1	0.78	0.19	0.19	0.17	0.17	0.30	-10.42	13
2	0.24	0.39	0.34	0.39	0.27	0.33	-9.76	10
3	0.22	**1.00**	**1.00**	**1.00**	**1.00**	**0.84**	**-1.48**	**1**
4	0.48	0.23	0.22	0.21	0.17	0.26	-11.64	17
5	0.65	0.21	0.20	0.19	0.18	0.29	-10.86	14
6	0.23	0.92	0.90	0.65	0.42	0.63	-4.08	2
7	0.86	0.21	0.21	0.17	0.17	0.33	-9.74	9
8	0.35	0.86	0.85	0.30	0.28	0.53	-5.55	6
9	0.69	0.20	0.19	0.18	0.17	0.29	-10.87	15
10	0.18	0.29	0.27	0.23	0.96	0.39	-8.26	7
11	**1.00**	0.17	0.17	0.17	0.17	0.33	-9.54	8
12	0.25	0.37	0.32	0.36	0.31	0.32	-9.78	11
13	0.82	0.72	0.66	0.63	0.17	0.60	-4.44	3
14	0.22	0.85	0.84	0.44	0.47	0.56	-4.97	5
15	0.38	0.20	0.20	0.18	0.17	0.23	-12.90	18
16	0.17	0.98	0.98	0.42	0.39	0.59	-4.64	4
17	0.73	0.23	0.22	0.19	0.17	0.31	-10.26	12
18	0.57	0.24	0.23	0.21	0.18	0.28	-10.91	16

Note: $^{0.2}$Weightage for each response is 0.2; SH: Shrinkage; WA: Water absorption; AP: Apparent porosity; BD: Bulk density; & FS: Flexural strength

Once the single performance property function was presented which were GRG values, the analysis was approaching traditional Taguchi design analysis, where it can be described by MINITAB 17 software. Response tables of grey relational grade is presented in Table 10, where it was highly influenced by sintering temperature parameter and it was followed by parameters of soaking time, composition of POFA, molding pressure, and type of POFA. These flows of significant level were previously recorded by single objective optimization of water absorption and apparent porosity. Meanwhile, Fig. 2 reports the main effect plot for SNR of GRG, where optimal parameters were as follows: 15 wt.% of UGPOFA, pressed at 2 t, sintered at 1200 °C, and 300 min of soaking times.

Table-10: Response tables of grey relational grade

Level	Design parameters (GRG)					Design parameters (SNR of GRG)				
	A	B	C	D	E	A	B	C	D	E
1	0.42	0.42	0.41	0.29	0.41	-8.27	-8.21	-8.19	-10.94	-8.28
2	0.40	0.43	0.39	0.36	0.38	-8.41	-8.15	-8.49	-9.25	-9.05
3	-	0.39	0.43	0.59	0.45		-8.66	-8.34	-4.83	-7.70
Delta	0.02	0.04	0.04	0.30	0.08	0.14	0.51	0.30	6.11	1.35
Rank	5	3	4	1	2	5	3	4	1	2

Note: GRG: Grey relational grade; SNR: Signal to noise ratio; A: Type of POFA; B: POFA composition; C: Molding pressure; D: Sintering temperature; E: Soaking time

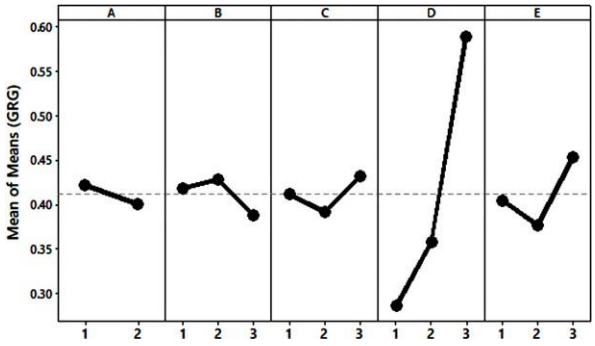

Fig.-2: Main effect plot for SNR of GRG.

3.3 Confirmation Experiment

The confirmation experiment is the final part of parametric design in the Taguchi design. It is performed to validate the developed optimal parameters, where difference of predicted and experimental values is reported. Table 11 records the result of confirmation experiment, where specimen for GRG was also included. SH, WA, AP, BD, and FS presents as optimal condition (single objective) for the best shrinkage, water absorption, apparent porosity, bulk density, and flexural strength, respectively. Meanwhile, GRG refers to a condition of multiple objective where it was termed as GRG. Experimental results from initial condition were described by a condition of No.1 specimen, where it presented the lowest value from each parameter. It was compared with experimental result of optimal condition. The results showed that optimal condition specimen have higher performance property values compared to initial condition.

Table-11: Result of confirmation experiment

Specimen	Performance properties	Initial condition	Optimum condition		
		Experimental	Predicted	Experimental	Difference
SH	Shrinkage (%)	2.59	1.21	1.48	0.27
WA	Water absorption (%)	15.44	2.03	1.76	0.27
AP	Apparent porosity (%)	28.04	4.49	4.01	0.48
BD)	Bulk density (g/cm^3)	1.83	2.28	2.37	0.09
FS	Flexural strength (MPa)	0.52	57.95	53.29	4.66
GRG	GRG	0.30	0.68	-	-
	Shrinkage (%)	2.59	NA	11.74	-
	Water absorption (%)	15.44	NA	2.47	-
	Apparent porosity (%)	28.04	NA	5.57	-
	Bulk density (g/cm^3)	1.83	NA	2.26	-
	Flexural strength (MPa)	0.52	NA	43.39	-

Note: NA- Not Applicable (Note: The prediction only for the GRG)

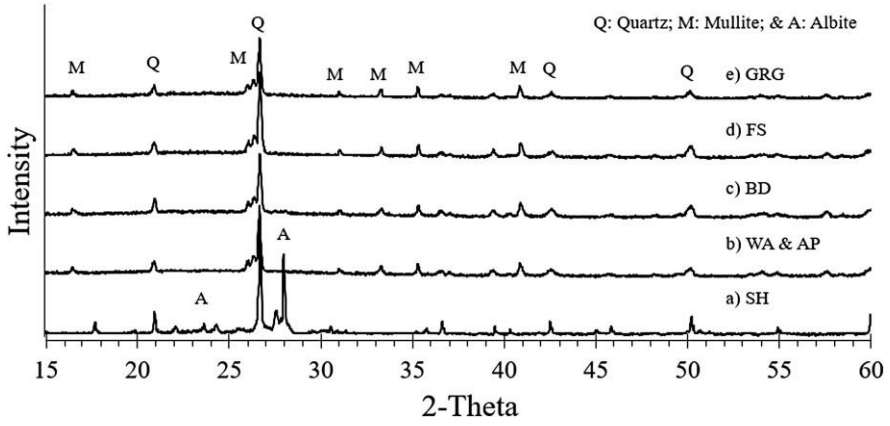

Fig.-3: XRD patterns of optimal specimens

The minor difference between predicted and experimental values was presented, where GRG specimen could not be recorded. Hence, it validated the optimal parameters developed. To enhance the developed optimal parameters,

optimal specimens were also validated by crystalline phase and morphology analyses. Fig. 3 records the results of crystalline phase analysis through XRD patterns. Generally, XRD pattern for SH specimen in Fig. 3(a) was observed to be different from other optimal specimens, where albite (00-009-0466) peaks were presented at 2Θ≈28°. However, it was prepared under a condition of 25 wt.% of UGPOFA, pressed at 3 t, sintered at 800 °C, and 60 min of soaking times. Previously, sintering temperature has assigned as the highest influence parameters, where 800 °C for optimal sintering temperature is the main reason for existing phases.

Other optimal specimens were presented by mullite phase (01-074-4146) peaks, where its developed sintering temperature was 1200 °C. The XRD results were minorly influenced by other parameters. For example, if SH specimen is ignored, XRD patterns for remaining optimal specimens would be similar although different optimal parameters are assigned. These crystalline phases were highly supported by morphology analysis, shown in Fig. 4. It had highly supported the crystalline phase that existed such as albite phase for SH specimen and mullite phase for remaining specimens.

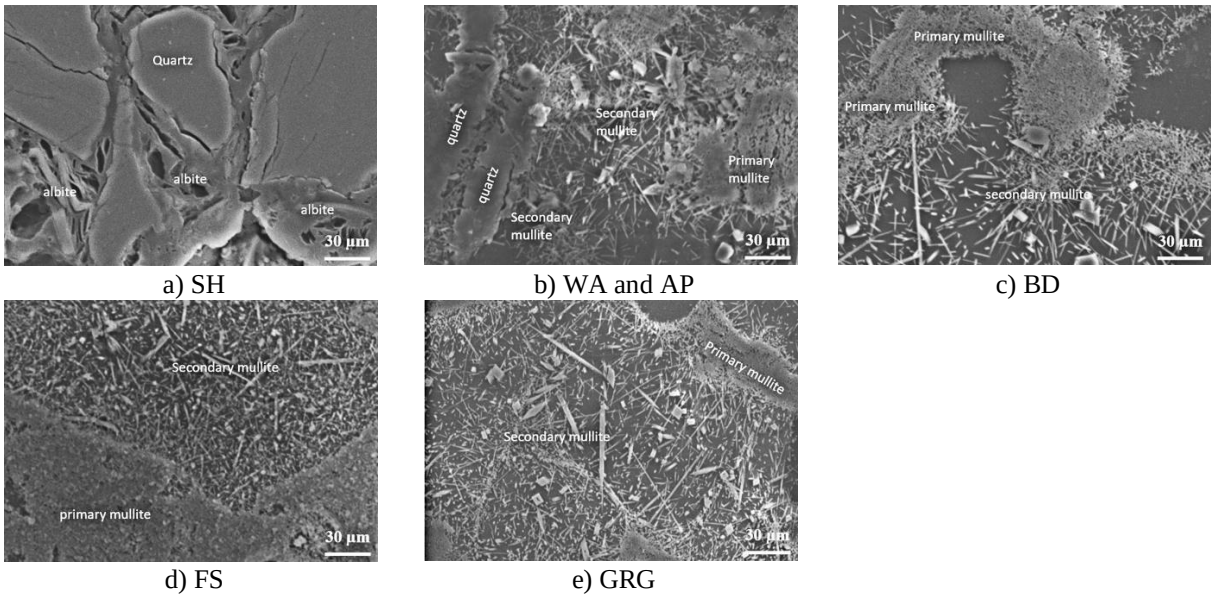

a) SH b) WA and AP c) BD

d) FS e) GRG

Fig. 4: Morphology analysis of optimal specimens

However, morphology analysis is enhanced by the formation of several types of mullite, where there is primary and secondary mullite. Theoretically, primary mullite is a form of decomposition of plastic material. Meanwhile, secondary mullite is a form from a reaction of flux agent and plastic material. However, secondary mullite can also be formed from a reaction of plastic material, flux agent, and filler material [49].Optimal specimens are mostly presented by UGPOFA except for BD and FS specimens. Because of the lowest influence parameters, there was no difference reported between optimal specimens. Meanwhile, 15 wt.% composition of POFA was most often recorded, where it was not recorded by SH and FS specimens. Previously, parameter for composition of POFA had ranked as the second or third influence parameters, where it might be causing few differences in its morphology analysis. The SH specimen was confirmed to generate different morphology analysis than other optimal specimens; however, no difference was observed for FS specimen unless in terms of mullite phase pattern. It means that FS specimen approach similar morphology analysis with WA, AP, and BD specimens. Region of primary and secondary mullite were clearly observed in FS specimen, where other optimal specimens were randomly presented. It means morphology images of WA, AP, and BD specimens are parallel with obtained property values. Moreover, it is also supported by its optimal parameter conditions.

4. Conclusion

This paper focuses on the chronological of Taguchi GRA method in application of triaxial ceramic by applying POFA. Investigated performance properties were shrinkage, water absorption, apparent porosity, bulk density, and flexural strength. Hence, six optimal specimens were recorded, where one set of optimal parameters was optimized in terms of multiple objectives. Sintering temperature was recorded as the highest influence parameters to all six objectives; while type of POFA was the least influence parameter.

The TGRA suggested the highest performances were obtained at this condition: 15 wt.% of UGPOFA, pressed at 2 t, sintered at 1200 °C, and 300 min of soaking times. Meanwhile, its performance properties were presented by 11.74% of shrinkage, 2.47% of water absorption, 5.57% of apparent porosity, 2.26 g/cm^3 of bulk density, and

43.39 MPa of flexural strength. The present study reported that both traditional Taguchi and Taguchi GRA were useful tools to optimize the process of triaxial POFA ceramic applying any waste materials.

Acknowledgement

This paper was partly sponsored by Centre for Graduate Studies, Universiti Tun Hussein Onn Malaysia.

Reference

[1] A. Zainudin, C.K. Sia, P. Ong, O.L.C. Narong, N.H.M. Nor, Taguchi design and flower pollination algorithm application to optimize the shrinkage of triaxial porcelain containing palm oil fuel ash, IOP Conf. Ser. Mater. Sci. Eng. 165 (2017) 12036.

[2] C.B. Carter, M.G. Norton, Ceramic Materials: Science and Engineering, Springer New York, 2007.

[3] E. Kamseu, C. Leonelli, D.N. Boccaccini, P. Veronesi, P. Miselli, G. Pellacani, U.C. Melo, Characterisation of porcelain compositions using two china clays from Cameroon, Ceram. Int. 33 (2007) 851–857.

[4] H. Boussak, H. Chemani, A. Serier, Characterization of porcelain tableware formulation containing bentonite clay, Int. J. Phys. Sci. 10 (2015) 38–45.

[5] M. Tarhan, B. Tarhan, T. Aydin, The effects of fine fire clay sanitaryware wastes on ceramic wall tiles, Ceram. Int. 42 (2016) 17110–17115.

[6] K. Kim, K. Kim, J. Hwang, Characterization of ceramic tiles containing LCD waste glass, Ceram. Int. 42 (2016) 7626–7631.

[7] M.F. Serra, M.S. Conconi, G. Suarez, E.F. Aglietti, N.M. Rendtorff, Volcanic ash as flux in clay based triaxial ceramic materials, effect of the firing temperature in phases and mechanical properties, Ceram. Int. 41 (2015) 6169–6177.

[8] Y. Luo, S. Zheng, S. Ma, C. Liu, X. Wang, Ceramic tiles derived from coal fly ash : Preparation and mechanical characterization, Ceram. Int. 43 (2017) 11953–11966.

[9] A. Álvaro Guzmán, S. Marisol Gordillo, A. Silvio Delvasto, V. María Francisca Quereda, V. Enrique Sánchez, Optimization of the technological properties of porcelain tile bodies containing rice straw ash using the design of experiments methodology, Ceram. Int. 42 (2016) 15383–15396.

[10] N.U. Kockal, Optimizing production parameters of ceramic tiles incorporating fly ash using response surface methodology, Ceram. Int. 41 (2015) 14529–14536.

[11] C. Jaturapitakkul, J. Tangpagasit, S. Songmue, K. Kiattikomol, Filler effect and pozzolanic reaction of ground palm oil fuel ash, Constr. Build. Mater. 25 (2011) 4287–4293.

[12] N.H.A. Khalid, M.W. Hussin, J. Mirza, N.F. Ariffin, M.A. Ismail, H.-S. Lee, A. Mohamed, R.P. Jaya, Palm oil fuel ash as potential green micro-filler in polymer concrete, Constr. Build. Mater. 102 (2016) 950–960.

[13] S.K. Lim, C.S. Tan, O.Y. Lim, Y.L. Lee, Fresh and hardened properties of lightweight foamed concrete with palm oil fuel ash as filler, Constr. Build. Mater. 46 (2013) 39–47.

[14] N. Mohamad, A.A.A. Samad, M.T. Lakhiar, O. Mydin, S. Jusoh, A. Sofia, S.A. Efendi, Effects of Incorporating Banana Skin Powder (BSP) and Palm Oil Fuel Ash (POFA) on Mechanical Properties of Lightweight Foamed Concrete, Int. J. Integr. Eng. 10 (2018) 69–76.

[15] N.O.L. Ching, S.C. Kiong, A. Zainudin, N.H.M. Nor, Y.S. Khee, C.K. Sia, A. Zainudin, N.H.M. Nor, S.K. Yee, Exploring the Potential of Palm Oil Fuel Ash (POFA) in EMI Shielding Effectiveness, J. Mech. Eng. 2 (2017) 101–111.

[16] O.L.C. Narong, C.K. Sia, S.K. Yee, P. Ong, A. Zainudin, N.H.M. Nor, N.A. Kasim, Optimization of the EMI shielding effectiveness of fine and ultrafine POFA powder mix with OPC powder using Flower Pollination Algorithm, IOP Conf. Ser. Mater. Sci. Eng. 165 (2017) 12035.

[17] O.L.C. Narong, C.K. Sia, S.K. Yee, P. Ong, A. Zainudin, N.H.M. Nor, M.F. Hassan, Optimization of EMI shielding effectiveness plaster mortar containing POFA using Taguchi design and Flower Pollination algorithm method, Int. J. Integr. Eng. 10 (2018) 93–101.

[18] O.L.C. Narong, C.K. Sia, S.K. Yee, P. Ong, A. Zainudin, N.H.M. Nor, M.F. Hassan, Optimisation of EMI shielding effectiveness: Mechanical and physical performance of mortar containing POFA for plaster work using Taguchi Grey method, Constr. Build. Mater. 176 (2018) 509–518.

[19] A. Zainudin, C.K.C.K. Sia, P. Ong, N.O.L.N.O.L. Ching, N.H.M.N.H.M. Nor, Potential of Palm Oil Fuel Ash (POFA) Layers as Secondary Raw Material in Porcelain Stoneware Application, J. Mech. Eng. 2 (2017) 71–81.

[20] R. K. Roy, Design of Experiment Using The Taguchi Method Approach, Wiley-Interscience, USA, 2001.

[21] G.S. Peace, Taguchi Methods : A Hands- On Approach, Addison-Wesley, 1993.

[22] S.N.A. Khalid, A.E. Ismail, M.H. Zainulabidin, A.M.T. Arifin, M.F. Hassan, M.R. Ibrahim, M.Z. Rahim, Mechanical Performances of Twill Kenaf Woven Fiber Reinforced Polyester Composites, Int. J. Integr. 10 (2018) 49–59.

[23] D. Jurków, J. Stiernstedt, Investigation of High Temperature Co-fired Ceramics sintering conditions using Taguchi Design of the experiment, Ceram. Int. 40 (2014) 10447–10455.

[24] M.J.A. Mijarsh, M.A. Megat Johari, Z.A. Ahmad, Synthesis of geopolymer from large amounts of treated palm oil fuel ash: Application of the Taguchi method in investigating the main parameters affecting compressive strength, Constr. Build. Mater. 52 (2014) 473–481.
[25] S. Chamoli, P. Yu, A. Kumar, Multi-response optimization of geometric and flow parameters in a heat exchanger tube with perforated disk inserts by Taguchi grey relational analysis, Appl. Therm. Eng. 103 (2016) 1339–1350.
[26] P.K. Sahu, S. Pal, Multi-response optimization of process parameters in friction stir welded AM20 magnesium alloy by Taguchi grey relational analysis, J. Magnes. Alloy. 3 (2015) 36–46.
[27] A.B. Shinde, P.M. Pawar, Multi-objective optimization of surface textured journal bearing by Taguchi based Grey relational analysis, Tribol. Int. 114 (2017) 349–357.
[28] A. Baruah, C. Pandivelan, A.K. Jeevanantham, Optimization of AA5052 in incremental sheet forming using grey relational analysis, Measurement. 106 (2017) 95–100.
[29] N. Senthilkumar, T. Tamizharasan, V. Anandakrishnan, Experimental investigation and performance analysis of cemented carbide inserts of different geometries using Taguchi based grey relational analysis, Measurement. 58 (2014) 520–536. doi:10.1016/j.measurement.2014.09.025.
[30] M.A. Salih, A.A. Abang Ali, N. Farzadnia, Characterization of mechanical and microstructural properties of palm oil fuel ash geopolymer cement paste, Constr. Build. Mater. 65 (2014) 592–603.
[31] N.H. Abdul Shukor Lim, M.A. Ismail, H.S. Lee, M.W. Hussin, A.R.M. Sam, M. Samadi, The effects of high volume nano palm oil fuel ash on microstructure properties and hydration temperature of mortar, Constr. Build. Mater. 93 (2015) 29–34.
[32] M.O. Yusuf, M.A. Megat Johari, Z.A. Ahmad, M. Maslehuddin, Influence of curing methods and concentration of NaOH on strength of the synthesized alkaline activated ground slag-ultrafine palm oil fuel ash mortar/concrete, Constr. Build. Mater. 66 (2014) 541–548.
[33] S. Akpinar, A. Evcin, Y. Ozdemir, Effect of calcined colemanite additions on properties of hard porcelain body, Ceram. Int. 43 (2017) 8364–8371.
[34] P.-T. Teo, A.A. Seman, P. Basu, N.M. Sharif, Recycling of Malaysia's electric arc furnace (EAF) slag waste into heavy-duty green ceramic tile., Waste Manag. 34 (2014) 2697–708.
[35] H. Wang, M. Zhu, Y. Sun, R. Ji, L. Liu, X. Wang, Synthesis of a ceramic tile base based on high-alumina fly ash, Constr. Build. Mater. 155 (2017) 930–938.
[36] J.M. Pérez, J.M. Rincón, M. Romero, Effect of moulding pressure on microstructure and technological properties of porcelain stoneware, Ceram. Int. 38 (2012) 317–325.
[37] J.M. Pérez, M. Romero, Microstructure and technological properties of porcelain stoneware tiles moulded at different pressures and thicknesses, Ceram. Int. 40 (2014) 1365–1377.
[38] H.U. Jamo, M.N. Maharaz, Influence of Mould Pressure and Substitution of Quartz by Palm Oil Fuel Ash on The Hardness of Porcelain Body, Sci. World J. 9 (2014) 23–28.
[39] A. Bernasconi, V. Diella, A. Pagani, A. Pavese, F. Francescon, K. Young, J. Stuart, L. Tunnicliffe, The role of firing temperature, firing time and quartz grain size on phase-formation, thermal dilatation and water absorption in sanitary-ware vitreous bodies, J. Eur. Ceram. Soc. 31 (2011) 1353–1360.
[40] ASTM C326, Standard Test Method for Drying and Firing Shrinkages of Ceramic Whiteware Clays, ASTM Int. (2003).
[41] ASTM C373, Standard Test Method for Water Absorption, Bulk Density, Apparent Porosity, and Apparent Specific Gravity of Fired Whiteware Products, Ceramic Tiles, and Glass Tiles, ASTM Int. (2014).
[42] ASTM C1161, Standard Test Method for Flexural Strength of Advanced Ceramics at Ambient Temperature, ASTM Int. (2003).
[43] A. Salem, S.H. Jazayeri, E. Rastelli, G. Timellini, Dilatometeric study of shrinkage during sintering process for porcelain stoneware body in presence of nepheline syenite, J. Mater. Process. Technol. 209 (2009) 1240–1246.
[44] T. Greenfield, A. V Metcalfe, Design and Analyse Your Experiment Using MINITAB, Wiley, 2009.
[45] S. Chitwaree, J. Tiansuwan, N. Thavarungkul, L. Punsukumtana, Energy saving in sintering of porcelain stoneware tile manufacturing by using recycled glass and pottery stone as substitute materials, Case Stud. Therm. Eng. 11 (2018) 81–88.
[46] X. Xi, L. Xu, A. Shui, Y. Wang, M. Naito, Effect of silicon carbide particle size and CaO content on foaming properties during firing and microstructure of porcelain ceramics, Ceram. Int. 40 (2014) 12931–12938.
[47] A.D.N. Junior, D. Hotza, V.C. Soler, E.S. Vilches, Effect of quartz particle size on the mechanical behaviour of porcelain tile subjected to different cooling rates, J. Eur. Ceram. Soc. 29 (2009) 1039–1046.
[48] M. Dal Bó, V. Cantavella, E. Sanchéz, F.A. Gilabert, A.O. Boschi, D. Hotza, An estimate of quartz content and particle size in porcelain tiles from young's modulus measurements, Ceram. Int. 43 (2017) 2233–2238.
[49] W.E. Lee, Y. Iqbal, Influence of mixing on mullite formation in porcelain, J. Eur. Ceram. Soc. 21 (2001) 2583–2586.